Journal of Power Sources 267 (2014) 171–181

Contents lists available at ScienceDirect

Journal of Power Sources

journal homepage: www.elsevier.com/locate/jpowsour

Use of mechanistic carbon corrosion model to predict performance loss in Polymer Electrolyte Membrane fuel cells

S.R. Dhanushkodi [a], S. Kundu [b], M.W. Fowler [a, *], M.D. Pritzker [a]

[a] Department of Chemical Engineering, University of Waterloo, Waterloo, ON N2G 3G1, Canada
[b] Automotive Fuel Cell Cooperation Corp., 9000 Glenlyon Parkway, Burnaby, BC V5J 5J8, Canada

HIGHLIGHTS

- Development of carbon corrosion testing protocols.
- Development of carbon corrosion model.
- Empirical correlation between carbon loss and performance loss.
- Prediction of performance loss of the MEA using carbon model.

ARTICLE INFO

Article history:
Received 25 October 2013
Received in revised form
28 April 2014
Accepted 7 May 2014
Available online 21 May 2014

Keywords:
Carbon corrosion
Kinetic model
Accelerated stress test
CAT cell
Carbon fingerprint

ABSTRACT

A membrane electrode assembly is subjected to carbon corrosion accelerated stress tests (ASTs) involving the application of square-wave voltage cycles with different upper limits to measure the resulting loss in the mass of the carbon support at the cathode catalyst layer (CL) and the associated degradation in performance. Carbon loss is determined from the amount of CO_2 evolved during degradation, while the performance loss is measured from the reduction in the cell voltage at 1.5 A cm^{-2} relative to the performance obtained in its beginning-of-life state. A kinetic model for carbon corrosion describing the rate of evolution of CO_2 is shown to accurately predict the carbon loss measured during the various carbon corrosion ASTs in this study. A plot of the performance losses from the various carbon corrosion ASTs versus the corresponding carbon losses reveals that all the data demonstrate consistent degradation regardless of the AST conditions, and these result can be fitted with an exponential function termed the 'fingerprint' expression. By combining the carbon corrosion model and fingerprint expression, both the carbon loss and performance loss of a cathode CL during a carbon corrosion AST can be accurately predicted based only on knowledge of the waveform of the input voltage.

1. Introduction

Transportation systems consume more than 20% of the world's total primary energy, produce 27% of total green-house emissions and operate at approximately 15% efficiency [1,2]. An advanced powertrain system such as a fuel cell system provides high quality power with significantly lower harmful emissions. Polymeric electrolyte membrane fuel cells (PEMFC) enable fast start-up, high efficiency and require relatively low maintenance compared to current automobiles that operate by the combustion of fossil fuels [3,4]. However, PEMFCs still face significant challenges related to material costs and durability that have impacted their commercialization. One of the factors limiting fuel cell durability is the corrosion of the carbon that supports the Pt catalyst, particularly at the cathode electrode. Carbon corrosion in PEMFCs is thermodynamically favorable over a wide range of cell voltages from 0.2 to 1.5 V [5,6]. This has been reported by a number of experimental studies. Corrosion of graphene-based carbons, such as carbon black, subjected to potential cycling has been shown to cause mass loss and surface oxide growth [7]. Carbon corrosion is also often observed to occur when the catalyst layer is partially covered by hydrogen and oxygen during startup/shutdown (SU/SD) cycling and when fuel starvation conditions prevail [6,8]. As with other processes, the kinetics of carbon corrosion depend on temperature, potential and duration of operation.

* Corresponding author.
E-mail address: mfowler@uwaterloo.ca (M. Fowler).

http://dx.doi.org/10.1016/j.jpowsour.2014.05.041
0378-7753/

A widely used approach to investigate carbon corrosion in PEMFCs is through the application of accelerated stress tests (ASTs) to mimic real-time operating conditions in automotive applications [7,9,10]. One of the most common such ASTs involves the application of a cell potential according to a square-wave waveform between a lower limit of 0.6–1.0 V and an upper limit of 1.2–1.55 V. The corrosion behavior of carbon is expected to change depending on a number of factors such as the upper/lower potential limits of the AST, catalyst loading, support loading and particle size.

To study commercial catalysts and their supports for PEMFCs, the use of mathematical models have also been helpful in gaining a better understanding of carbon oxidation and its reaction mechanism. Many carbon corrosion models either completely neglect the complex behavior observed or are based on empirical equations for the mass loss of the electrode [11]. However, such models are poor at predicting mass loss and surface oxide concentrations for different oxidation conditions. A better approach has been to develop physicochemical models describing the various phenomena leading to the corrosion of the carbon support. Meyers et al. developed a mathematical model for carbon corrosion due to hydrogen cross-over that induces both oxygen evolution and carbon corrosion at the cathode under fuel-starved conditions [12,13]. Franco and Gerard proposed a mechanistic model describing the coupling between the electrocatalysis of the oxygen reduction reaction (ORR) in the membrane electrode assembly (MEA) and corrosion of the cathode carbon support [14]. Their numerical simulations indicated that cathode thickness and cell potential decrease when the anode chamber is partially exposed to oxygen due to hydrogen cross-over or fuel starvation. Their model-predicted carbon loss arises by oxidation of carbon by electrocatalytic mechanisms. Gallagher and Fuller proposed a model based on an electrochemical mechanism to predict carbon weight loss and surface oxide growth as a function of time, temperature and potential [15,16]. According to this mechanism, the following phenomena contribute to current decay during electrochemical oxidation: carbon mass loss due to CO_2 formation, reversible formation of a passive carbon oxide on the surface and irreversible formation of another carbon oxide. Comparison of model predictions with experimental data indicates that the current decay occurring when the cathode potential is held constant at 1.2, 1.3 and 1.4 V_{SHE} can be attributed to the formation of the reversible passive oxide. On the other hand, when the potential is cycled, the irreversible loss of the oxide intermediate that catalyzes CO_2 formation through quinones formation was found to be the most significant cause of current decay.

The physicochemical model proposed by Gallagher and Fuller provides considerable insight into carbon corrosion occurring during ASTs, but includes several complex intermediate steps in the overall reaction mechanism and so may be difficult to implement for online monitoring and analysis of carbon corrosion ASTs in practical situations [15]. Furthermore, it is not possible to conduct experiments that can identify and distinguish between the various surface oxides proposed in the model. Thus, a number of the quantities predicted by the model are not experimentally observable. A simpler model capable of tracking the oxidation of the carbon during potential cycling would make it easier to interpret AST data and develop strategies to mitigate catalyst layer degradation and/or more accurately predict the lifespan of fuel cell stacks.

One of the main objectives of this study is to fit a kinetic model to the carbon loss measured during carbon corrosion and mixed degradation ASTs. Ultimately the resulting model used in this work is a simplified version of the corrosion model proposed by Gallagher and Fuller [15]. A sensitivity analysis of the contributions of the various reaction steps to the measured electrode responses is employed to determine whether simplification of this model can be satisfactorily made. In theory, fuel cell performance loss due to carbon corrosion should be correlated to the amount of carbon loss. However, the model of Gallagher and Fuller is unable to predict the performance loss such as the decrease in cell voltage from knowledge of the carbon loss. Thus, in order to more closely link the data collected from ASTs to fuel cell performance loss and gain a better understanding of the contributions of the different modes of carbon corrosion to this loss, it would be very useful to incorporate a correlation between performance loss and carbon loss into the Gallagher and Fuller model (or some simplified version). This would enable a direct link to be made between the operating conditions during ASTs and the resulting carbon and performance losses. Ultimately, this would enable better diagnose of the causes of performance loss during normal fuel cell operation, design of Pt/C catalysts and strategies to extend the useful lifetimes of MEAs. Consequently, another important aspect of this study is to develop an empirical relation or an observable performance indicator or 'fingerprint' between the measured performance loss and the carbon loss predicted by the kinetic model for each AST. Comparisons of the performance losses obtained from this fingerprint equation to those determined experimentally are made to validate this approach.

2. Experimental

The cell operating conditions for the different experiments conducted in this study are given in Table 1. The sequence of steps followed for each MEA that is subjected to an accelerated stress test protocol is: i) MEA preparation, ii) conditioning of the MEAs, iii) measurement of electrochemical platinum surface area (EPSA) using cyclic voltammetry analysis, iv) measurement of a polarization curve using current sweep method, v) accelerated stress test vi) cell recovery and vii) CO_2 measurement. The details involved in each experimental step are discussed below.

2.1. MEA preparation

The Pt catalyst used at the cathode in the MEAs was obtained from TKK Corp. The MEAs tested consisted of graphitic carbon-supported platinum (40 wt% platinum) layers and membranes based on perfluorosulfonic acid (PFSA). The Pt loading levels at the cathode were 0.4 mg cm^{-2}. The catalyst-coated membrane and gas diffusion media were cut using a swing beam cutting press, aligned precisely with frames and bonded to make a MEA with active superficial area of 48.4 cm^2. Once an MEA was assembled in the cell hardware, a leak test was done. A pressurized bladder was used to press the MEA against the conducting flow-field plates in order to improve fuel cell performance. The optimal bladder pressure was determined based on the performance of the cell for each assembly. Generally, the bladder pressure was maintained between 60 and 80 psi.

Table 1
Operating conditions for experiments investigating carbon corrosion.

	Conditioning	Polarization	CV	ASTs	Recovery
Load (A cm^{-2})	2.0	0–2.4	0	0	0
Temperature (°C)	70	60	60	70	70
Fuel/oxidant gas	H_2/air	H_2/air	H_2/N_2	H_2/N_2	H_2/N_2
Fuel/oxidant pressure (barg)	1.7/1.5	1.7/1.5	1.5/1.5	1.5/1.5	0.4/0.03
Fuel/oxidant flowrate (slpm)	2/8	2/12	2/12	1/1	1/0
Fuel/oxidant RH (%)	100/100	100/100	100/100	100/100	50/50

2.2. Cell conditioning

The MEAs used in the carbon corrosion AST experiments were conditioned for 12 h at a constant current density of 2.0 A cm^{-2}, 100% RH and 70 °C with the hydrogen and air flow rates maintained at 2 and 8 slpm, respectively. The conditions during the testing are listed in Table 1. After conditioning, the fuel cell was purged with N_2 for 15 min before beginning the electrochemical experiments to evaluate the beginning of life (BOL) performance.

2.3. Cyclic voltammetry (CV)

To assess the changes in the electrochemical platinum area (EPSA) during ASTs, CVs were obtained at 60 °C using accepted procedures. CO stripping CV analysis was done to measure the electrochemical surface area (ECSA) during the carbon corrosion studies. The CVs during the carbon corrosion studies were measured using an in-house built set-up assisted by a load bank. The conditions used for these CV measurements are given in Table 1. The ECSA (cm^2 g^{-1}) was determined using the expression below [17]:

$$\mathrm{ECSA} = Q_{CO}/0.484\,[\mathrm{Pt}] \quad (1)$$

where [Pt] represents the platinum loading (mg cm^{-2}) at the cathode, Q_{CO} the area (mC cm^{-2}) under the CO stripping region during the anodic sweep of the CV and 0.484 mC cm^{-2} corresponds to the charge density required to oxidize a monolayer of CO on the Pt surface [18]. The formula given in Eq. (1) is based on the assumption that one CO atom covers one Pt atom. The catalyst loading at the cathode was set to 0.4 mg-Pt cm^{-2} throughout this study. Once the ECSA was determined, EPSA was computed using the following expression [11,17]:

$$\mathrm{EPSA} = 10\,L_w U_{Pt} \mathrm{ECSA} \quad (2)$$

where L_w is the catalyst loading and U_{Pt} is the Pt utilization at the cathode. A value of 0.8 for U_{Pt} was assumed based on Neyerlin et al. [19].

2.4. Polarization measurements

To characterize the performance losses in this study, polarization curves were obtained under identical conditions at regular intervals during each AST. The conditions used to obtain these polarization curves during ASTs are given in Table 1. A steady state polarization curve was measured using H_2 and air as the fuel and oxidant at flow rates of 2 slpm and 10 slpm, respectively, and operating at 100% RH and 60 °C at both the anode and cathode. To obtain each point on the polarization curve, the steady state cell voltage was obtained at each applied current density over the range from 2.4 A cm^{-2} down to 0 A cm^{-2}. Before each polarization curve was determined, the fuel cell was operated at 1.7 A cm^{-2} for 20 min to ensure that the system was initially in a stable state. Performance loss was determined from the polarization curve using Equation (3) below:

$$\text{Voltage decay rate} = \frac{E_{\mathrm{BOL}_{@1.5\ \mathrm{A\ cm^{-2}}}} - E_{\mathrm{after}\ n\ \mathrm{cyles}_{@1.5\ \mathrm{A\ cm^{-2}}}}}{n\ \text{cycles}} \quad (3)$$

2.5. ASTs

Carbon corrosion ASTs were conducted by applying square-wave pulses with different upper potential and lower potential limits to the cell operated with H_2 fed on the anode side and N_2 on the cathode side. The pulses shown in Fig. 1 include: i) square-wave voltage cycles between 1.0 V and 1.42 V, ii) square-wave voltage cycles between 1.0 V and 1.44 V, iii) square-wave voltage cycles between 1.0 V and 1.468 V, iv) square-wave voltage cycles between 1.0 V and 1.48 V, v) square-wave voltage cycles between 1.0 V and 1.5 V and vi) square-wave voltage cycles between 1.0 V and 1.4 V. In the first five cases, these pulses were applied with dwell times of 5 s and 5 s at the lower and upper potentials. Dwell times of 30 s and 30 s were used in the sixth AST. The carbon corrosion rate at the cathode is expected to rise when the upper voltage during ASTs is raised above 1.4 V. However, if the upper limit becomes too high, severe damage to the cell and its performance can occur. Accordingly, a range of upper limits between 1.4 and 1.5 V was chosen for these ASTs as a compromise to promote carbon corrosion but not cause excessive degradation. All ASTs were applied for 2500 cycles.

In addition to the carbon corrosion ASTs, square-wave voltage cycles between 0.6 V and 1.4 V with dwell times of 30 s and 30 s, respectively, were applied to the MEAs to impose mixed Pt dissolution-carbon corrosion conditions. Due to more extensive degradation of the MEAs, this AST was terminated after 1500 cycles instead of 2500 cycles.

2.6. Recovery

After completion of a specified number of cycles during an AST, the load bank was turned off and the cathode was purged with N_2 at a rate of 1 slpm for 20 min. This procedure was aimed at removing excess water present in the catalyst layer [20].

2.7. CO_2 measurement

Throughout each AST experiment, the carbon dioxide content in the exhaust gas was measured using a Model 100 Infrared Analyzer (California Analytical Instruments). The amount of carbon lost due to corrosion was determined from this measurement. These ASTs have been chosen so that carbon corrosion occurs primarily in the cathode catalyst layer. Carbon corrosion of other PEM fuel cell components such as the gas diffusion layer (GDL), membrane and the flow field were investigated separately, which were found to be negligible during these ASTs. Due to commercial confidentiality, these results are not presented in this article.

3. Carbon corrosion model

Not surprisingly, the extent of cathode carbon support corrosion and the consequential performance loss during ASTs and typical fuel cell operation is strongly affected by the operating conditions. The most comprehensive model to date for the kinetics of carbon corrosion in fuel cell catalyst layers developed by Gallagher and Fuller [15] describes the formation of CO_2 and a number of surface carbon oxides and determines the electrode response, carbon weight loss and surface oxide growth during the electrochemical oxidation of graphitic carbon as a function of time, temperature and potential. A key feature of their proposed mechanism is the existence of two types of sites on the carbon support surface. One type of site is active for the rate-determining step of CO_2 formation, while the other type is involved both in CO_2 formation and the formation of various carbon oxides on the support surface [15,16].

In all experimental studies, the extent of carbon corrosion is determined from the loss of carbon mass during the ASTs which can be based entirely on measurements of the amount of CO_2 formed. The first half of the mechanism proposed by Gallagher and Fuller describes the formation of CO_2, while the second half involves the

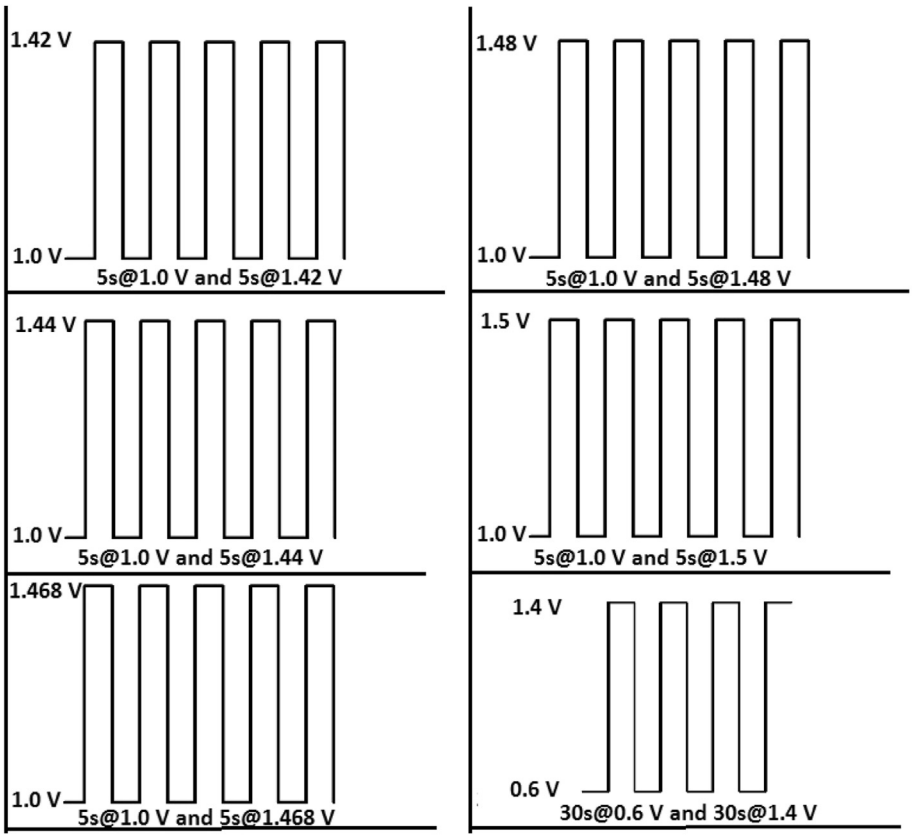

Fig. 1. AST voltage cycles used to develop and assess carbon corrosion model.

formation of the surface oxides. However, the identification of the particular surface oxides formed on the carbon support and determination of the amounts present are difficult tasks, particularly if they are to be done on a routine basis during MEA design and/or monitoring fuel cell operation. Consequently, the portion of the reaction mechanism proposed by Gallagher and Fuller that is most relevant to the analysis of the ASTs in the present study is the first half describing CO_2 formation. For these reasons, it seems reasonable to investigate whether the carbon loss during the ASTs can be satisfactorily predicted by a simplified version of Gallagher and Fuller model involving the formation of CO_2, not including the degradation associated with that of the formation of surface oxides. Consequently, we have conducted a sensitivity analysis to determine whether the complete Gallagher and Fuller model can be simplified in this way without any adverse effect on its accuracy. This involves assessing the simplified model by comparing its predictions to those of the full Gallagher and Fuller model for conditions described in the original study [15].

The reaction steps involved in the formation of CO_2 that constitutes the simplified mechanism are given below. According to the mechanism, the carbon surface contains two types of sites denoted as # and *. Those designated as # are active sites for the rate-determining step, while * sites are the location of both CO_2 generation and the formation of the surface carbon oxides.

$$C^{\#} + H_2O \rightarrow C^{\#}OH + H^+ + e^- \quad (4)$$

$$C^{\#} + H_2O \leftrightarrow C^{\#}(H_2O)_{ads} \quad (5a)$$

$$C^{\#}(H_2O)_{ads} + C^{\#}OH \rightarrow C^{\#}OC^{\#}OH + 2H^+ + 2e^- \quad (5b)$$

$$2C^{\#}OC^{\#}OH + 3C^{*} + 3H_2O \rightarrow C^{*}O(C^{*}OOH)_2 + 2C^{\#} + 2C^{\#}OH + 4H^+ + 4e^- \quad (5c)$$

$$C^{*}O(C^{*}OOH)_2 \rightarrow C^{*}OOH + C^{*}O + * + CO_2 + H^+ + e^- \quad (5d)$$

$$C^{*}OOH \rightarrow * + CO_2 + 4H^+ + 4e^- \quad (5e)$$

The number designation for these steps given here is the same as that defined by Gallagher and Fuller [15]. The process begins with the oxidation of # sites to form a $C^{\#}OH$ surface oxide (Equation (4)) and the reversible adsorption of water on other # sites to form $C^{\#}(H_2O)_{ads}$ (Equation (5a)). These two surface species combine together to form a $C^{\#}OC^{\#}OH$ intermediate in Equation (5b) which is the slowest and rate-determining step for CO_2 formation. The $C^{\#}OC^{\#}OH$ intermediate then goes on and begins a sequence of anodic oxidation steps (Equations (5c)–(5e)) that yields CO_2. The subsequent steps in the full model proposed by Gallagher and Fuller make up a competing pathway that leads to the reversible formation of carbon oxide $C_x^{\#}O$ and to the irreversible formation of$C_x^{\#}O_3$, quinone ($C_x^{\#}O_2$) and hydroquinone $C_x^{\#}(OH)_2$. These are not considered in the simplified model.

The calculation of the carbon loss is the same in both the full and simplified models. A material balance on the moles of carbon N_c yields the following equation for the instantaneous rate of change of carbon mass [16]:

$$\frac{\partial N_c}{\partial t} = -r_2\, SMN_c \quad (6)$$

where N_c is number of moles of carbon present per unit geometric area (mol cm_{geom}^{-2}), r_2 is the rate of formation of CO_2 (mol $cm^{-2}\ s^{-1}$),

S is the specific surface area ($cm^2\ g^{-1}$) of the carbon determined from BET measurement and M is the molecular weight of carbon ($g\ mol^{-1}$). A couple of points are worth noting regarding the use of r_2 in Equation (4). First, r_2 is the combined rate of steps 2a–e in the model and represents the overall rate of generation of CO_2. Secondly, as noted above, the carbon loss during oxidation can only be measured from the amount of CO_2 that is formed. Consequently, only r_2 is used in Equation (4). For the purposes of this analysis, it suffices to present the rate expressions for Equations (4) and (5) that comprise the proposed simplified model:

$$r_1 = k_1\theta_{vac}\exp\left[\frac{\alpha_1 F}{RT}(V-U_1) - g\theta_{C^{\#}OH}\right] \quad (7)$$

$$r_2 = k_2\theta_{vac}\theta_{C^{\#}OH}\left(\frac{p_0}{p_0^{ref}}\right)\exp\left[\frac{\alpha_2 F}{RT}(V-U_2)\right] \quad (8)$$

$$k_i = k_i^0\exp\left[-\frac{E_{a,i}}{RT}\right] \quad (9)$$

where r_i is the rate ($mol\ cm^{-2}\ s^{-1}$) of reaction i, θ_{vac} is the fraction of surface sites that are vacant or free, $\theta_{C^{\#}OH}$ is the fraction of sites covered by $C^{\#}OH$, V is the electrode potential (V) on the standard hydrogen scale, p_0 is the partial pressure (kPa) of water vapor and p_0^{ref} is a reference pressure (270 kPa) for water vapor. The other parameters in these expressions are: equilibrium potential U_i(V), transfer coefficient α_i, activation energy $E_{a,i}$ ($J\ mol^{-1}$), pre-exponential rate constant k_i^0 ($mol\ cm^{-2}\ s^{-1}$) and rate constant k_i ($mol\ cm^{-2}\ s^{-1}$) for reaction i, Frumkin factor g, Faraday constant F (96485.3 C mol^{-1}), gas constant R (8.314 J $mol^{-1}\ K^{-1}$) and temperature T(K). r_2 is equivalent to the rate of step 2b which is rate-determining. Since step 2a is assumed to be much faster than step 2b, it is considered to be at pseudo-equilibrium and the equilibrium constant for step 2a is incorporated within the rate constant k_2 appearing in Equation (6). The Frumkin factor g was set equal to three by Gallagher and Fuller since this value gave the best fit of their model to the experimental data.

A balance on the total number of rate of generation of $C^{\#}OH$ sites on the surface yields:

$$\frac{\partial\theta_{C^{\#}OH}}{\partial t} = \frac{r_1 - r_2}{[\#]} \quad (10)$$

Since # sites are either vacant or occupied by $C^{\#}OH$ sites, then

$$[\#] = [\#]_{vac} + [C^{\#}OH] \quad (11)$$

$$1 = \theta_{vac} + \theta_{C^{\#}OH} \quad (12)$$

where $\theta_{vac} = [\#]_{vac}/[\#]$ and $\theta_{C^{\#}OH} = [C^{\#}OH]/[\#]$.

The concentration of the active reaction sites [#] and the specific surface area S depend on the original carbon black material used and the subsequent heat treatment in an argon atmosphere prior to incorporation into the MEA. Both of these quantities can be estimated from knowledge of the temperature of this heat treatment step. To estimate the concentration of total active sites on the carbon support, the following empirical function reported by Gallagher and Fuller is used [15]:

$$[\#] = 70.3\exp(-0.0075\ T_{heat\ treatment}) \quad (13)$$

where [#] is given in units of $mol\ m^{-2}$. S was found by Gallagher and Fuller to vary linearly with the heat treatment temperature and can be obtained from a plot presented in their paper (Fig. 8 in Ref. [15]). Since Gallagher and Fuller fitted their model to data collected on carbon that had been heat treated at 2173 K, [active sites] and S are set to 5.88×10^{-6} $mol\ m^{-2}$ and 100 $m^2\ g^{-1}$, respectively, for the purpose of assessing the accuracy of the simplified model. It should be noted that the carbon supports used in the present study were heat treated at 2200 °C. Thus, different values of [active sites] and S are used when the carbon corrosion model is applied to the experimental data obtained during the ASTs of the present study. S is obtained using BET analysis. The equilibrium potential U_2 of step 2 depends on temperature according to the following expression used by Gallagher and Fuller [15]:

$$U_2 = -0.00023T + 0.2326{**}S{**} \quad (14)$$

All the electrochemical parameter values used in the simplified carbon model are the same as those obtained by Gallagher and Fuller [15] and are given in Table 2. The carbon surface is assumed to be completely unoxidized at the outset of each AST before cycling. With the parameters and initial conditions specified, the simplified carbon model represented by Equations (4)–(12) can then be solved. The complete set of rate expressions constituting the full model for comparison can be found in the paper by Gallagher and Fuller [15].

4. Results and discussion

4.1. Accuracy of the simplified model

To assess the accuracy of the simplified model, comparisons were made between the simulations of the electrode response to various ASTs using this model to that obtained using the full model. Fig. 2a shows the predictions of the two models on the evolution of the carbon mass loss over the course of an AST in which the cell voltage is held fixed at 1.4 V. Model simulation was done for 18 h of operation by keeping the cell potential constant at 1.4 V hold at 60 °C for H_2 and N_2 conditions. Although the curve obtained using the simplified model does not perfectly overlay that of the full model, the difference is very small even after 18 h. Comparisons of predictions by the two versions of the model for other conditions showed similar good agreement.

Fig. 2b shows a comparison of the corresponding values of $\theta_{C^{\#}OH}$ over the course of the constant voltage-AST at 1.4 V predicted by the simplified and complete models. Once again, good agreement between the two versions of the model is obtained. The rate of carbon loss is beginning to tail off near the end of the 1.4 V hold AST (Fig. 2a), whereas the coverage of active sites is accelerating at the end. This growth in $\theta_{C^{\#}OH}$ shows that the rate at which it is being consumed is falling behind its rate of production.

Fig. 3 shows the predictions of the two models on the evolution of the carbon mass loss over the course of an AST 1.0–1.5 V 5 s/5 s. Model simulation was carried out for 2000 cycles of operation. The curve obtained using the simplified model is in good agreement

Table 2
Parameters used in fitting the simplified model to experimental data.

Parameters	Symbol	Value	Units
Transfer coefficient of step 1	α_1	0.35	No units
Transfer coefficient of step 2	α_2	0.65	No units
Activation energy for step 1	$E_{a,1}$	10	kJ mol^{-1}
Activation energy for step 2	$E_{a,2}$	110	kJ mol^{-1}
Rate constant for step 1	k_1	2.35×10^{-16}	mol $cm^{-2}\ s^{-1}$
Rate constant for step 2	k_2	9.50×10^{-3}	mol $cm^{-2}\ s^{-1}$
Equilibrium potential of step 1	U_1	1	V
Equilibrium potential of step 2	U_2	0.15	V

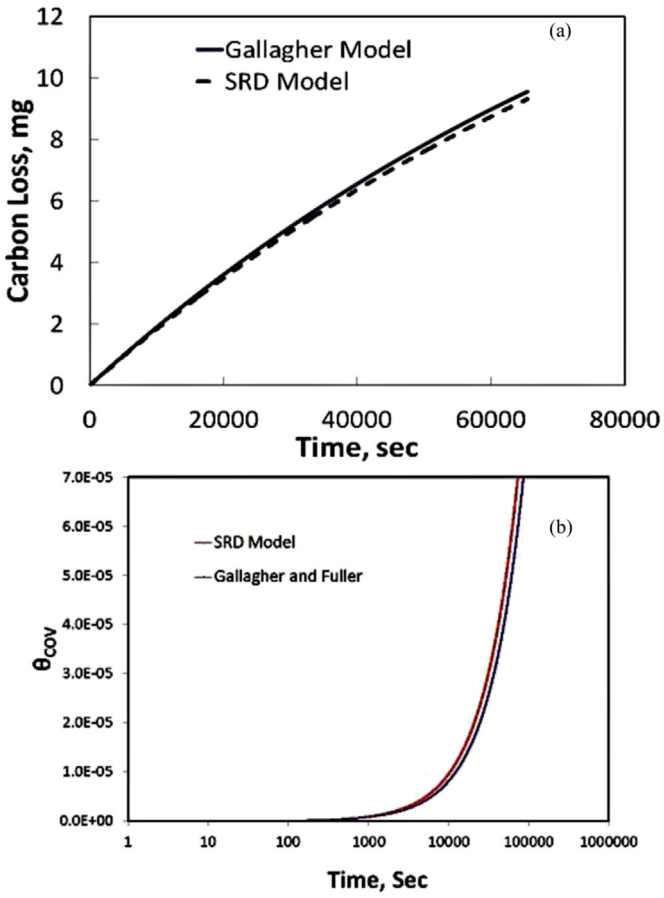

Fig. 2. (a) Comparison of the evolution of carbon loss during an AST in which the cell voltage is held constant at 1.4 V computed using the full Gallagher and Fuller model [13] and the simplified model presented in this study. (b) Variation in COH sites during AST of 1.4 V hold as computed by the simplified carbon corrosion model presented in this study.

with the full Gallgher and Fuller model. Based on these comparisons, one can conclude that the simplified model is accurate enough for use in analyzing the carbon corrosion ASTs of the current study.

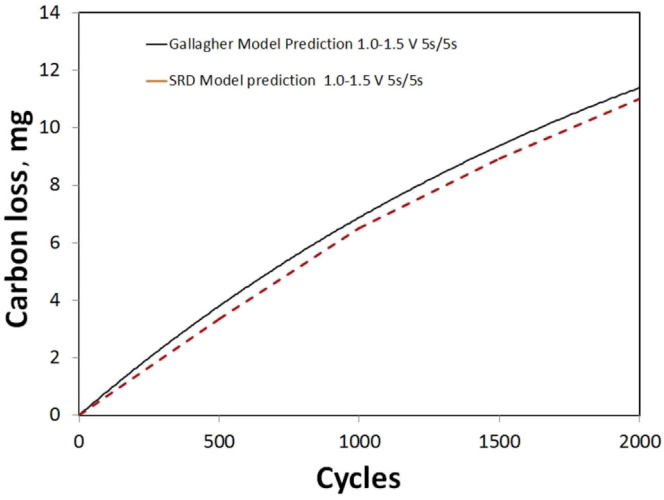

Fig. 3. Comparison of the evolution of carbon loss during an AST in which the cell voltage is cycled between 1.0 and 1.5 V after every 5 s computed using the Gallagher and Fuller model [13] and the simplified model presented in this study.

4.2. Validation of carbon loss measurement for different ASTs

Carbon loss measured during different ASTs is presented in Fig. 4a. In order to validate the simplified model against experimental data, the carbon loss measured during AST involving square-wave cycles between 1.0 and upper limits ranging from 1.42 V to 1.5 V with 5 s/5 s dwell times is plotted in Fig. 4a along with the losses obtained using the model for the identical condition. It is important to emphasize that all model parameter values are identical to those reported by Gallagher and Fuller [15] or are adjusted in the case of [#] (Equation (11)), S and U_2 (Equation (12)) to account for the fact that the heat treatment step used to prepare the carbon support in the current study was carried out at 2200 °C. Thus, the computed curves are obtained without any fitting of the simplified model to the experimental data and so represent true predictions of the model. It should be noted that the excellent agreement between the computed and the experimentally measured carbon losses of the current study is obtained despite the fact that the MEA considered in the current study differs from that used by Gallagher and Fuller. The model and the associated parameter values in Table 2 thus appear to be robust enough to accurately predict the carbon loss due to carbon corrosion independently of the particular MEA in question. To simulate the other ASTs, the input into the model is the upper electrode potential V that is varied with time so as to match the appropriate waveform shown in Fig. 1. With V specified, the model is then solved numerically to yield the cumulative carbon loss. The results of each

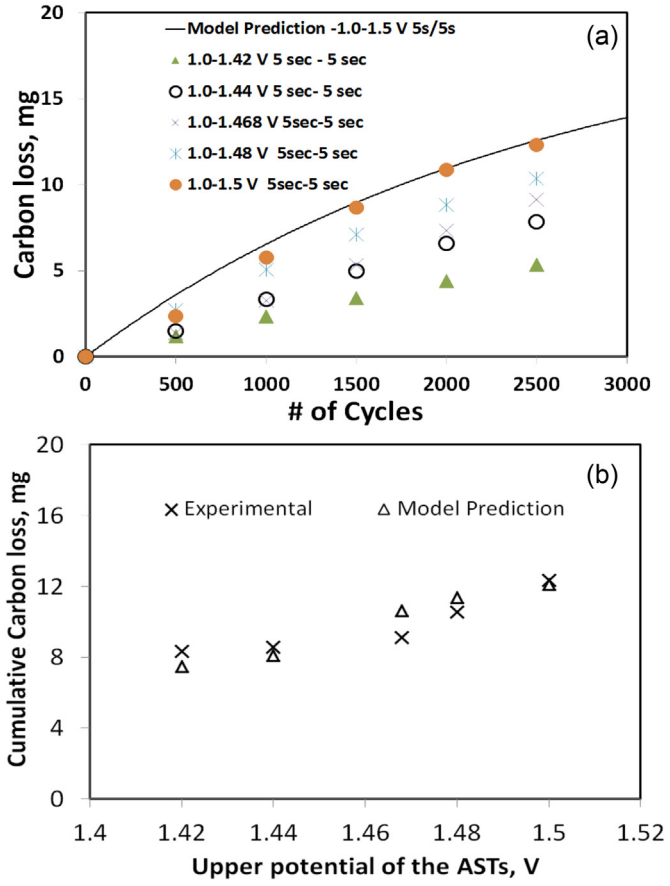

Fig. 4. (a) Carbon loss measured during different ASTs. (b) Variation of the total carbon loss with the upper potential limit of the ASTs as determined from experiments and the carbon corrosion model of this study. Reported total carbon loses are for a MEA that consists active area of 48.4 cm^2.

ASTs are presented in Fig. 4b and show excellent agreement between the experimental and computed cumulative carbon loss.

A particularly striking aspect of the results presented in Fig. 4b is the effect that the upper limit of the square-wave voltage cycles has on carbon loss. The lower limit (1.0 V) and dwell times (5 s/5 s) are identical for these five ASTs. They differ only with regard to the upper limit, which varies over the narrow range from 1.42 to 1.5 V. A relatively small increase from 1.42 V to 1.5 V more than doubles the carbon loss at comparable points throughout the AST. Repeated cycling of the potential of the fuel cell cathode above 1.0 V promotes the corrosion of the carbon support. The carbon losses reported here are similar in magnitude to those reported by Linse et al. who subjected cathode layers to ASTs with lower potential of 1.0 V and upper potentials ranging from 1.2 to 1.5 V [5]. Experimental results reported by Linse et al. [5] and others [3,4] indicate that non-catalyzed oxidation of a significant portion of the carbon on the catalyst layer surface occurs during the ASTs and that some of the remaining carbon tends to agglomerate and shrink. Although carbon corrosion is the predominant mode of degradation during these ASTs, a small amount of dissolution of the Pt catalyst likely also occurs when the potential is cycled above 1.0 V [12,21].

A *t*-test and analysis of variance (ANOVA) have been applied to the carbon loss data measured during these ASTs and obtained from the simplified model to determine whether the differences between the two sets are statistically significant. Since each experiment was repeated three times, triplicate data were obtained for each measurement and used for the statistical analysis. A minimum of 25 data points were used to test the hypothesis. The results of these analyses for the various ASTs are presented in Table 3. The $t_{critical}$ value is obtained from a *t*-table for $\alpha = 0.05$ [22]. When the magnitude of $t_{statistic}$ obtained from a *t*-test is found to be smaller than $t_{critical}$, the analysis indicates that the differences between the experimental and model data are not statistically significant. F_{obs} values are obtained from the ANOVA by calculating the ratio between the variance between groups and the variance within the groups for each AST. The critical value $F_{critical}$ is obtained from an F-table for $\alpha = 0.05$. A finding of $F_{obs} > F_{critical}$ signifies that the differences between the experimental and model data are not statistically significant. Both the *t*-tests and ANOVA yield very similar results. As shown in Table 3, the conditions $t_{statistic} < t_{critical}$ and $F_{obs} > F_{critical}$ are easily met in all of the carbon corrosion ASTs of this study, indicating no statistically significant differences between the experimental and model data in any of these cases. Only in the case of the AST involving square-wave cycles between 0.6 V and 1.4 V with 30 s/30 s dwell times are these conditions found not to be satisfied. However, such an observation is perfectly reasonable since Pt dissolution as well as carbon corrosion should occur during these cycles, unlike the other ASTs listed in Fig. 1 where carbon corrosion is predominant. Since the model accounts for carbon corrosion only, a finding that no statistically significant difference exists between the experimental data and model predictions for the 0.6–1.4 V AST would in fact have been problematic. In summary, these statistical analyses provide further evidence of the suitability of the simplified model to predict the carbon loss measured during the carbon corrosion ASTs.

Table 3
t-test and ANOVA analyses of the simplified carbon corrosion model.

AST	*t*-test		ANOVA	
	$t_{statistic}$	$t_{critical}$ $\alpha = 0.05$	F_{obs}	$F_{critical}$ $A = 0.05$
1.0–1.4 V, 30 s/30 s	0.04	2.3	88.47	9.55
1.0–1.42 V, 5 s/5 s	0.42	2.3	49.31	9.55
1.0–1.44 V, 5 s/5 s	0.02	2.3	51.74	9.55
1.0–1.468 V, 5 s/5 s	−0.15	2.3	57.70	9.55
1.0–1.48 V, 5 s/5 s	−0.23	2.3	49.23	9.55
1.0–1.5 V, 5 s/5 s	−0.13	2.3	100.96	9.55
0.6–1.4 V, 30 s/30 s	2.3	2.3	9.23	9.55

4.3. Performance loss during the carbon corrosion ASTs

The maximum current density measured during polarization curve measurement during ASTs is found to be ~2.0 A cm^{-2}. The performance loss of the MEA during the ASTs is characterized in terms of the voltage loss obtained at an applied current density of 1.5 A cm^{-2}. At this current density, activation, ionic, electronic and contact resistances play a role in determining cell performance, whereas mass transport effects are relatively unimportant.

The evolution of the performance loss during the various ASTs is plotted against the number of cycles in Fig. 5a. This data shows that the upper potential limit during the ASTs does not affect the performance loss as strongly as it influences the carbon loss (Fig. 5a) except when 1.48 and 1.5 V are reached. The degradation in performance remains relatively modest (less than 60 mV) over the entire AST of 2500 cycles as long as the upper limit remains below ~1.47 V. However, with any further increase in the upper limit, the losses begin to grow dramatically, particularly after 2000 cycles. The decay in potential reaches 150 mV after 2500 cycles when the upper limit is raised to 1.48 V and as much as 625 mV with a further increase in the upper limit to 1.5 V. This last case is quite striking since a performance loss of 625 mV represents 82% of the initial BOL cell voltage observed at 1.5 A cm^{-2}. As shown in Section 4.2, the loss of carbon does not significantly affect the performance loss during the initial stages of these carbon corrosion ASTs. However, as the number of cycles increases beyond 1500, the impact on the performance loss becomes much larger.

4.3.1. Use of carbon corrosion fingerprint in the simplified model

Performance loss is generally caused by both Pt dissolution and carbon corrosion [12,16,23,24]. However, oxidation of the carbon support is expected to be the major contributor to performance loss during the carbon corrosion ASTs of this study due to the specific operating conditions employed. Young et al. postulated that the complete or partial oxidation of carbon to CO_2 during the ASTs affects the catalyst layer structure and presumably the porosity of the CL [25]. Recently, an empirical correlation of observed performance changes or a 'fingerprint' in the form of an exponential function relating performance loss to the carbon loss at a specific current density was developed in an earlier work and found to fit the data very well [26]. For an MEA of a particular type or structure, the same fingerprint is found to apply regardless of the AST. This expression enables the performance loss to be predicted from knowledge of the carbon loss. Although useful, this approach has at least one disadvantage. Development of the fingerprint expression requires the simultaneous and independent measurements of both the amount of CO_2 generated and performance loss. The CO_2 measurement requires that the cell be connected to an infrared instrument for continuous in-situ analysis, which is not always convenient or possible, particularly for routine monitoring of fuel cell performance during typical operation. However, it should be possible to eliminate the need for such a measurement by replacing it with the carbon corrosion model presented here that is able to determine the carbon loss as a function of time or the number of cycles during the ASTs. In this way, only a polarization measurement which can be easily conducted in-situ during ASTs or fuel cell operation is required.

To illustrate this approach, the performance loss measured at 1.5 A cm^{-2} is plotted versus the corresponding carbon loss of the MEA for all the carbon corrosion ASTs of this study in Fig. 5b. The

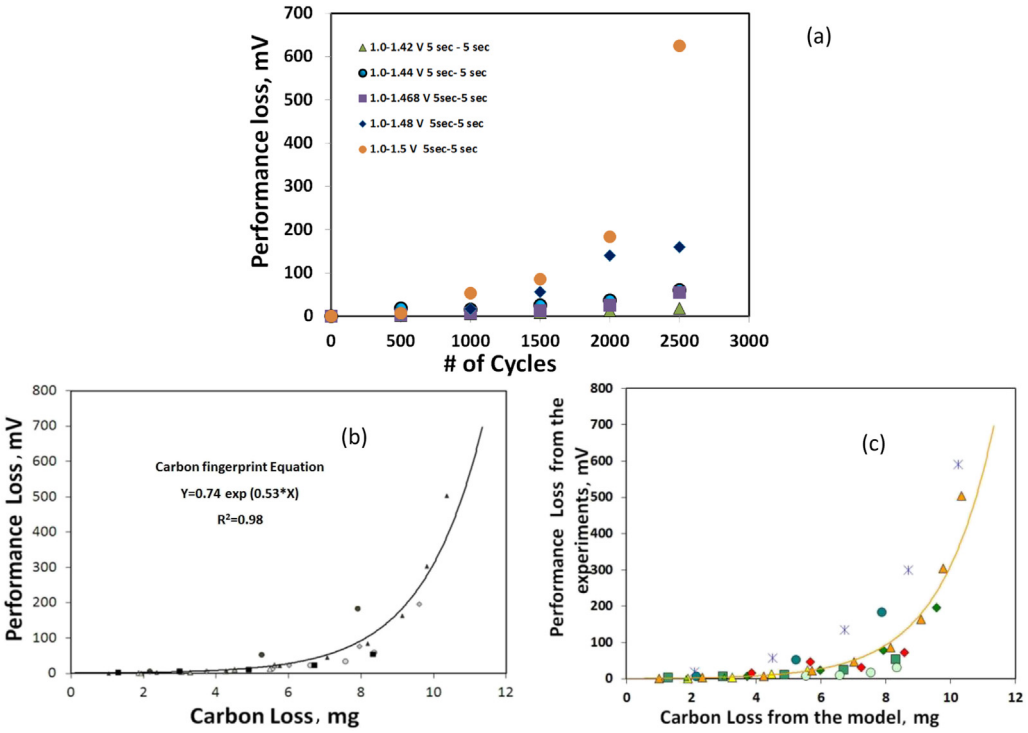

Fig. 5. (a) Performance loss measured during the course of the carbon corrosion ASTs. Relation between performance loss and carbon loss measured at 1.5 A cm^{-2} during carbon corrosion ASTs as determined directly from (b) experiments (symbols) and (c) simplified carbon model.

carbon loss data plotted along the *x*-axis in Fig. 5a are experimental values, while those appearing in Fig. 5b are computed values from the carbon corrosion model. The plots in Fig. 5b and c appear very similar, which is not surprising given that the predictions of the carbon corrosion model agree very well with the experimental data. Another important and useful feature of these plots is that the data for the various ASTs appear to fall along single curves despite the fact that the upper potentials differ, similar to the trend reported in our previous study [26]. This observation provides another indication that carbon corrosion is the predominant mode of cathode CL degradation during these ASTs. It also suggests that the change of the upper potential limit during these ASTs primarily affects the extent of the damage to the CL rather than to the nature of the degradation. An exponential function relating performance loss to carbon loss has been fit to the combined data from all of the ASTs to yield the solid curves in Figs. 5b and c. The exponential functions which this work terms fingerprint expressions are given in the figure legend. Very good agreement with the model predicted and experimentally determined cumulative performance loss is observed for all ASTs (Fig. 6). Although not included here, a *t*-test and ANOVA carried out on the experimental and model fitted data in Fig. 6 indicate that the differences between the measured and fitted performance loss have no statistical significance.

The observation that the same fingerprint expression is obtained regardless of the particular carbon corrosion AST being applied simplifies the analysis of CL degradation. As described previously, the carbon loss values on the solid curve in Fig. 5c are not measured and instead are computed by the carbon corrosion model. Thus, by combining the fingerprint expression with the carbon corrosion model, both the performance loss and carbon loss at any time during an AST can be predicted just from knowledge of the input voltage waveform without the need for any experiments. It must be acknowledged that the analysis presented in this communication has been restricted to a MEA of a particular type prepared using a given procedure. Although not included here, experiments were conducted on another MEA containing the same catalyst and loading level, but the MEA differed in other respects (i.e., GDL material, layer construction, ionomer/carbon ratio, temperature of heat treatment of carbon support). Interestingly, the results reveal that the simplified carbon corrosion model and associated parameters presented here are robust enough to accurately predict the carbon loss of this MEA as well during the ASTs. However, they also show that the fingerprint expression that accurately describes its corresponding performance loss differs from that of the other MEA type. Based on this finding, performance loss measurements should therefore be carried out to determine the fingerprint expression for a particular MEA type, but no further

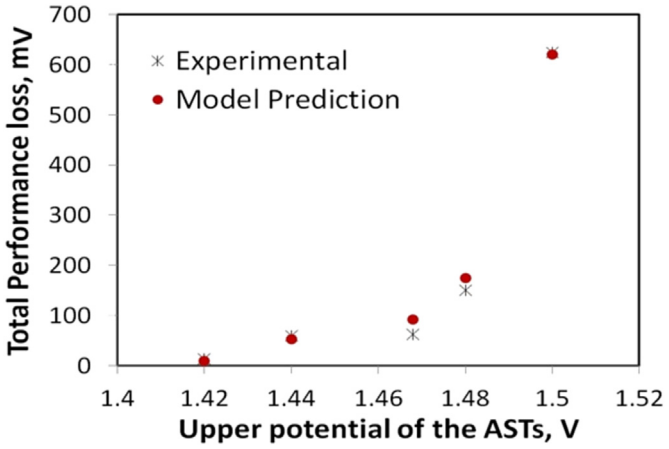

Fig. 6. Experimentally observed and predicted total performance for different upper potentials of the carbon corrosion ASTs obtained at 1.5 A cm^{-2}. Measured and predicted total carbon loses are for a MEA that has active area of 48.4 cm^2.

experiments would be required once a fingerprint expression has been established. However, since only two MEA types have been tested in this work, it will be important in the future to extend this study to a thorough investigation of MEAs having different designs, fabrication procedures, and structures (e.g., GDL material, layer construction, ionomer/carbon ratio, catalyst type, catalyst loading level, temperature of carbon support heat treatment) and determine whether their carbon loss during the ASTs can also be accurately predicted by the simplified carbon corrosion models with the parameters presented here.

4.4. Model applicability to mixed-mode degradation AST

The sensitivity of the carbon corrosion model and fingerprint equation developed previously [24] is assessed by applying it to an experiment involving a mixed-mode degradation AST during which both Pt dissolution and carbon corrosion operate. This AST consists of square-wave voltages cycles between 0.6 and 1.4 V with 30 s dwell times at each potential. The variation of the measured carbon loss over the course of this AST is presented in Fig. 7a. Comparison with the carbon ASTs results shown in Fig. 4a indicates that the application of this mixed-mode degradation AST leads to much higher carbon losses than do the carbon corrosion ASTs (with the exception of the AST between 1.0 and 1.5 V) despite the fact that the upper limit of 1.4 V is lower than the others and only 1500 cycles have been applied. Fig. 7a shows a comparison of the measured carbon loss to that predicted by the simplified carbon corrosion model. It should be noted that the model parameters have been left unchanged from those used to analyze the carbon corrosion ASTs and no attempt have been made to change the parameters to fit the model to the experimental data. The model underestimates the amount of carbon lost by an amount that grows over the course of the AST. This result is understandable given that the model accounts for only CO_2 formation during carbon oxidation and ignores catalyst-induced effects [5]. Furthermore, the trends shown in Fig. 7a suggest that the effects of Pt dissolution compared to carbon loss grows over the course of the AST. The relation between the corresponding performance loss measured during the AST and the carbon loss is plotted in Fig. 7b. Also included is the predicted behavior obtained using the fingerprint expression obtained (Fig. 5c) previously from the carbon corrosion ASTs. As with the carbon losses, the predictions underestimate the measured performance losses.

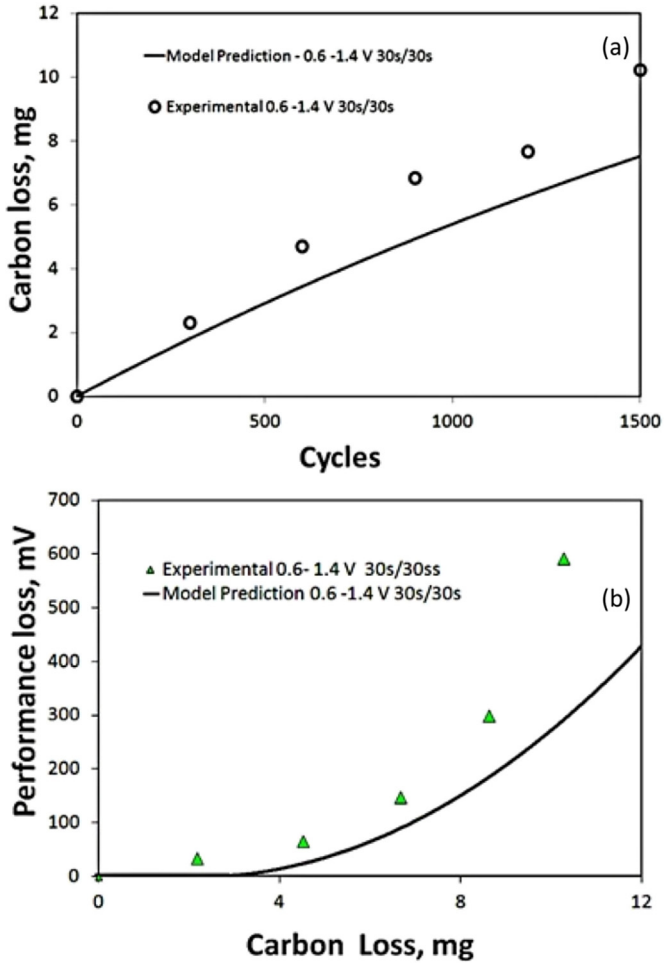

Fig. 7. (a) Variation of the measured and model-predicted carbon loss with number of cycles for a MEA contains active area of 48.4 cm^2 and (b) variation of the measured and model-fitted performance loss with carbon loss during the mixed-mode degradation AST (0.6–1.4 30 s/30 s AST).

Another possible cause of the underestimation by the simplified model is that it does not account for the formation of quinone/hydroquinone species and surface oxides during potential cycling [6,12,15,16,27]. Although not included here, we also conducted simulations of the full carbon corrosion model proposed by Gallagher and Fuller that account for these reactions, and found that it also under-predicts the observed carbon losses. Furthermore, the simplified model is able to accurately predict the carbon loss during the carbon corrosion ASTs which have the same or a higher upper voltage limit than that of the mixed-mode degradation AST. Previously reported studies indicate that Pt likely has a stronger effect on carbon corrosion during cycles from 0.6 V to 1.4 V than during cycles from 1 V to 1.4 V. Maass et al. observed increased carbon corrosion due to changes in the catalytic activity of platinum in the potential range of 0.6–1.0 V [27]. Linse et al. suggested that the oxidation state of platinum can strongly influence carbon corrosion [5]. Takeuchi et al. investigated carbon corrosion under dynamic potential conditions and also showed that the presence of Pt affects carbon oxidation at potentials below 1 V [28].

Information on the effect that Pt has on carbon corrosion can be gained by measuring the loss of EPSA during the carbon corrosion and mixed-mode degradation ASTs. Fig. 8a shows the relation between % carbon loss and % EPSA loss during the various ASTs. A strong correlation exists between these two quantities and both increase together during any given AST. Furthermore, the relation between % carbon loss and % EPSA loss for each AST is almost linear. A linear dependence during the carbon corrosion ASTs would be expected assuming that the Pt catalyst is uniformly distributed over the carbon support. Furthermore, if the Pt catalyst were to become detached and electrochemically disconnected from the fuel cell circuit as the carbon is oxidized to CO_2, one would expect this line to lie close to the 45° diagonal. The data obtained during most of the carbon corrosion ASTs lie above the diagonal line, suggesting that when carbon is oxidized to CO_2 some of the catalyst attached to it remains in electrochemical contact. An exception to this trend is observed in the case of the 1.0 V–1.4 V 30 s/30 s AST where the data fall somewhat below the diagonal, suggesting that some direct attack of the catalyst may be occurring. It is also observed that a change in the upper voltage limit during the carbon corrosion ASTs has a significant effect on the amount of carbon that is oxidized, but much less influence on the loss of % EPSA. The curve for the mixed-mode degradation AST lies well below the diagonal, reflecting that a considerable amount of the attack occurs directly on the catalyst without oxidizing the support.

An interesting comparison can be made between the % carbon loss and % EPSA loss during the mixed-mode degradation AST and

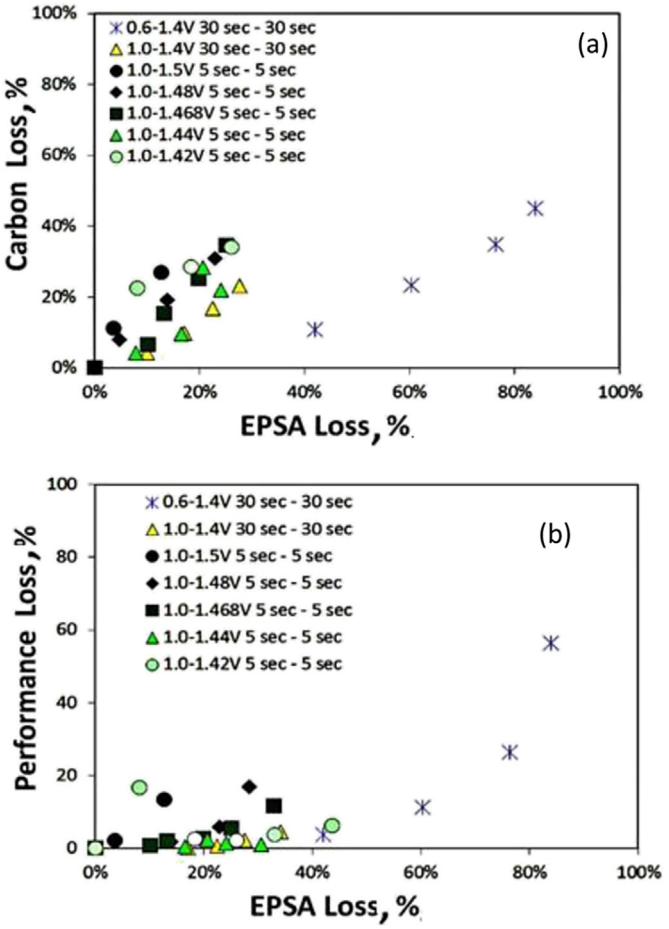

Fig. 8. Correlation between (a) % carbon loss and % EPSA loss and (b) % performance loss and % EPSA loss measured during carbon corrosion and mixed degradation ASTs. Operating conditions during these ASTs are given in Table 1.

that during the carbon corrosion AST. Although care must be taken in doing so on the basis of most of the carbon corrosion ASTs in Fig. 8a, due to differing dwell times; however, a clear comparison can be made with the results obtained during the 1.0 V–1.4 V 30 s/30 s AST where the dwell times are the same. Overall, both the % EPSA loss and % carbon loss vary over much wider ranges and reach much higher levels when the MEA is subjected to the mixed degradation AST than to the 1.0 V–1.4 V 30 s/30 s AST. The much higher % EPSA loss during the mixed-mode degradation AST than during the carbon corrosion AST is not surprising although the observation that it grows to a level above 80% is worth noting. Somewhat more surprising is the observation that the corresponding % carbon losses during the mixed-mode degradation ASTs are also much higher than those during the carbon corrosion AST. While the % carbon loss by the end of the 1.0 V–1.4 V 30 s/30 s AST of 2500 cycles reaches 22%, as much as 45% of the carbon is lost by the end of the 0.6 V–1.4 V 30 s/30 s AST which is carried out for only 1500 cycles. Obviously, these effects can be attributed to processes occurring at potentials below 1.0 V.

Particularly interesting are the trends observed when comparisons are made over the course of the two ASTs. Whereas the carbon loss levels are similar in the earlier stages of both ASTs, the corresponding EPSA loss of 40% during the 0.6 V–1.4 V 30 s/30 s AST is more than double the level reached during the 1.0 V–1.4 V 30 s/30 s AST. This, of course, reflects the particular attack on the Pt catalyst during this stage of the mixed-mode degradation AST. As the 0.6 V–1.4 V 30 s/30 s AST proceeds, the degradation of the catalyst continues, but so does that of the carbon support. The carbon loss of ~20% reached when the EPSA loss rises to ~60% matches the maximum level reached during the 1.0 V–1.4 V 30 s/30 s carbon corrosion AST. Thereafter, both the Pt catalyst and carbon support continue to degrade until the AST is terminated. The fact that the carbon loss is significantly higher than that observed during the carbon corrosion AST by the end of the cycling suggests that the attack on Pt also tends to enhance carbon corrosion either directly or indirectly.

The % performance loss, corresponding to the % carbon loss shown in Fig. 8a, is plotted versus % EPSA loss in Fig. 8b. Interestingly, the % performance loss tends to lag behind the % EPSA loss and % carbon loss throughout the carbon corrosion and mixed-mode degradation ASTs. Perhaps the most significant observation regarding the carbon corrosion ASTs is that the loss in performance always remains small (10% or less) even when the carbon loss and EPSA loss become substantial. This trend is even more remarkable during the earlier stages of the mixed-mode degradation AST. For example, even when 60% of the EPSA and 25% of the carbon have been lost, the performance is only diminished by 10%. However, thereafter the situation changes dramatically and the performance begins to deteriorate much more rapidly with further degradation of the support and catalyst so that the losses reached during the later stages of this AST are much greater than those during the carbon corrosion ASTs.

5. Conclusions

The durability of an MEA has been investigated by subjecting it to carbon corrosion ASTs with different upper potential limits and cycling periods and then measuring the resulting carbon loss and performance loss. Carbon loss is measured from the amount of CO_2 evolved during degradation, while the performance loss is determined from the decrease in the cell voltage at 1.5 A cm^{-2} relative to that obtained in its BOL state. A kinetic model for carbon corrosion based on the simplification of a mechanism reported in the literature has been found to accurately predict the carbon loss measured during the various carbon corrosion ASTs considered in this study. When the performance losses from the various carbon corrosion ASTs are plotted together versus the corresponding carbon losses, all the data fall along a single universal curve regardless of the AST. An exponential function termed the fingerprint expression has been fit to this curve and found to describe the correlation very well. By combining the carbon corrosion model and fingerprint expression, it is possible to accurately predict both the carbon loss and performance loss of a cathode CL subjected to a carbon corrosion AST from knowledge of the input voltage waveform alone.

Acknowledgments

The authors are grateful to the Natural Sciences and Engineering Research Council of Canada (NSERC Grant Number : RGPIN-261669-2008) for funding support to carry out this research. They also acknowledge the NSERC Industrial Postgraduate Scholarship (NSERC – IPS) program and AFCC for providing a scholarship for one of the authors (SRD). Preliminary model analysis done by Rosanna Yee, AFCC is much appreciated.

References

[1] L. Hockstad, B. Cook, in: P.A. U.S. Environmental Protection Agency, National Service Center for Environmental Publications, Washington, DC, 2012.

[2] S.R. Dhanushkodi, N. Mahinpey, A. Srinivasan, M. Wilson, J. Environ. Informatics 11 (2008) 36–44.
[3] S.R. Dhanushkodi, S. Kundu, M. Fowler, M. Pritzker, J. Power Sources (2013).
[4] S.R. Dhanushkodi, M. Fowler, A. Mazza, M. Pritzker, in: Proton Exchange Membrane Fuel Cells: Contamination and Mitigation Strategies, vol. 151, CRC press, 2010 (Chapter 4).
[5] N. Linse, L. Gubler, G.G. Scherer, A. Wokaun, Electrochim. Acta 56 (2011) 7541–7549.
[6] N. Linse, G.G. Scherer, A. Wokaun, L. Gubler, J. Power Sources (2012).
[7] K. Kinoshita, Carbon: Electrochemical and Physicochemical Properties, first ed., John Wiley Sons, New York, NY, 1988.
[8] J.H. Kim, E.A. Cho, J.H. Jang, H.J. Kim, T.H. Lim, I.H. Oh, J.J. Ko, I.J. Son, J. Electrochem. Soc. 157 (2010) B118–B124.
[9] K.H. Kangasniemi, D. Condit, T. Jarvi, J. Electrochem. Soc. 151 (2004) E125–E132.
[10] L. Roen, C. Paik, T. Jarvi, Electrochem. Solid-State Lett. 7 (2004) A19–A22.
[11] R. Makharia, S. Kocha, P. Yu, M.A. Sweikart, W. Gu, F. Wagner, H.A. Gasteiger, ECS Trans. 1 (2006) 3–18.
[12] J.P. Meyers, R.M. Darling, J. Electrochem. Soc. 153 (2006) A1432–A1442.
[13] J. Meyers, in: Modeling and Numerical Simulations, vol. 43, Springer, New York, 2009, pp. 249–271.
[14] A.A. Franco, M. Gerard, J. Electrochem. Soc. 155 (2008) B367–B384.
[15] K.G. Gallagher, T.F. Fuller, Phys. Chem. Chem. Phys. 11 (2009) 11557–11567.
[16] K. Gallagher, R. Darling, T. Fuller, in: Handbook of Fuel Cells, 2010.
[17] H.A. Gasteiger, S.S. Kocha, B. Sompalli, F.T. Wagner, Appl. Catal. B Environ. 56 (2005) 9–35.
[18] H. Gasteiger, W. Gu, R. Makharia, M. Mathias, B. Sompalli, Beginning of Life MEA Performance—Efficiency Loss Contributions, Wiley Online Library, 2003.
[19] K. Neyerlin, W. Gu, J. Jorne, H.A. Gasteiger, J. Electrochem. Soc. 153 (2006) A1955–A1963.
[20] X. Cheng, Z. Shi, N. Glass, L. Zhang, J. Zhang, D. Song, Z.S. Liu, H. Wang, J. Shen, J. Power Sources 165 (2007) 739–756.
[21] N. Takeuchi, T.F. Fuller, J. Electrochem. Soc. 155 (2008) B770–B775.
[22] J. Cohen, Statistical Power Analysis for the Behavioral Sciences, Routledge, 1988.
[23] J.D. Fairweather, B. Li, R. Mukundan, J. Fenton, R.L. Borup, ECS Trans. 33 (2010) 433–446.
[24] M. Wesselmark, C. Lagegren, G. Lindbergh, ECS Trans. 25 (2009) 1241–1250.
[25] A. Young, J. Stumper, E. Gyenge, J. Electrochem. Soc. 156 (2009) B913–B922.
[26] S.R. Dhanushkodi, M. Tam, S. Kundu, M.W. Fowler, M.D. Pritzker, J. Power Sources 240 (2013) 114–121.
[27] S. Maass, F. Finsterwalder, G. Frank, R. Hartmann, C. Merten, J. Power Sources 176 (2008) 444–451.
[28] N. Takeuchi, T.F. Fuller, ECS Trans. 25 (21) (2009) 1045–1054.